Theoretical Analysis of the Impact of IBRs on Impedance Trajectories during Power Swings

Sachintha Kariyawasam and Athula Rajapakse

***Abstract*--Despite their numerous advantages, abundant presence of IBRs in power systems causes a multitude of issues to conventional power system protection and operation. The work presented in this paper studies the effects on IBRs on power swing impedance trajectories by generic theoretical examination using phasor domain equations. A well-established model used for analyzing power swing phenomena was modified appropriately to incorporate IBRs. Phasor domain equations for the new power swing model with an IBR were derived and validated through EMT simulations. Using the derived model, power swing trajectory under various conditions were analyzed and the potential impacts of IBR on power swing protection were discussed. The work demonstrates that simplified, generic theoretical examination can provide useful information about impedance trajectories during power swings.**

***Keywords*: Inverter-based Resources, Power swing, Power system protection, Out-of-step protection.**

I. Introduction

POWER swings originate due to major system disturbances such as loss of large generation or load that cause abnormal oscillations in the power flow. Protection devices, impedance-based relays in particular, are prone to interpret these events as faults, prompting undesired tripping. Line protection relays are often provided with out-of-step (OOS) or power swing protection schemes which counter such eventualities through power swing blocking (PSB) or out-of-step tripping (OST) functions [1]-[5]. PSB is used for distinguishing power swings from faults and OST is used for separating stable power swings from unstable ones (where generators slip poles). In majority of line protection relays, OOS protection functions are based on the apparent impedance. PSB generally measures the time taken for the impedance observed at relaying point to travel from one region on the R-X (Resistance-Reactance) plane to another and commonly referred to as blinder schemes. The principle behind this is that the rate of change of swing impedance is slugging as it is restrained by the system inertia. In comparison, impedance change during a fault is almost instantaneous with signal processing in the relay adding a delay of around one cycle for detection. Once a power swing is detected, OST is triggered when the swing impedance enters a predefined zone, which is based on the least stable power swing characteristic [1]-[5].

Typically, inverter-based resources (IBR) provide limited rotational inertia to the connected power system, due to the decoupling caused by power electronic converters [6]-[10]. As a result, power swing characteristics of a power system alters with IBR penetration. Studies have shown that due to increased levels of IBR penetration, swing impedances move faster due to the lack of inertia of the system, and PSB timer settings calculated without accounting for this fact may be too high to distinguish between a fault and a stable power swing [6]-[9]. Lowering the PSB timer setting is the obvious remedy for this issue, but it is challenging to select this value in a way that the dependability of fault detection is not affected.

Typically, dynamics of synchronous machine controls such as exciters are ignored during power swing protection as they are deemed too slow to react during the first swing [11]. The behavior of an IBR control system during a power swing can be fundamentally different than that of a synchronous machine [6], and some control functions of a modern IBR, such as those applicable to voltage-ride through (VRT) requirements can respond in a much quicker time-frame (performance requirements for current injection during VRT mode ≤ 4 cycles as per IEEE Std. 2800-2022 [12]). This is a relatively unexplored topic worthy of further investigation.

Several recent publications discuss the impact of IBRs on power swing protection [7]-[10], [13]-[15]. Most of them, however, focus on the effect of IBRs' lack of inertia on the rate-of-change of the apparent impedance (the speed of the swing trajectory) during a power swing. A rigorous analysis of the impact of IBRs on impedance swing trajectories is largely absent in literature. References [6]-[10] analyze how replacing synchronous generation with IBRs can affect the dynamics of power swing in a system, primarily using simulation results. Work presented in [13] had derived a dynamic model for power swings for systems with IBRs and, it has been utilized in [14] to study practical implications on power swing protection. While this work had produced an in-depth investigation and detailed modelling, it requires complex system models, thus cannot be conveniently adopted. The premise of most previous studies is that faster moving swing impedances due to decreased system inertia may cause difficulty in distinguishing power swings and system faults. Moreover, the results presented indicate that the introduction of IBRs may alter the boundary between stable and unstable power swings, warranting revaluation of power swing protection settings (OST blinders in particular). Reference [8] briefly mentions the effect of IBR controls on swing trajectories, however, only very limited details are provided on this matter. The work of [15] presents a theoretical analysis of IBRs' effect on power swing impedance

(e-mail of corresponding author: kapugesk@myumanitoba.ca).
S. Kariyawasam and A. Rajapakse are with the Department of Electrical and Computer Engineering, University of Manitoba, Canada.

Paper submitted to the International Conference on Power Systems Transients (IPST2025) in Guadalajara, Mexico, June 8-12, 2025.

trajectories, taking control dynamics of IBRs into account. However, the investigation was carried out on a single-source-to-infinite-bus system, where the source is an IBR. While this represents an important development, the configuration considered does not represent a common situation where the power swing protection is critical. Therefore, further investigations for more generic configuration are warranted.

Main goal of this paper is to investigate the effects of IBRs on power swing impedance trajectories using a generic circuit equivalent, without resorting to complex dynamic models. Analysis of traditional power swing protection is generally carried out using simplified system equivalents represented in phasor domain, and the work presented in this paper attempt to incorporate IBRs into this type of simple analysis. Thus, the presented phasor domain analysis is based on well-established principles, modified to incorporate IBRs. This type of analysis does not intend to address the effect of IBR on the swing speed due to reduced inertia, which has been adequately investigated in literature. As a secondary objective, the impact of potential changes to swing trajectories on traditional power swing protection are also examined. In addition, the proposed method also provided a vital point of reference against which results from more detailed simulation can be compared.

The rest of this paper is organized as follows. Section II provides a theoretical analysis of power swing impedance trajectories in the presence of an IBR, which is validated by EMT simulation in Section III. Using the theoretical premise presented, results for different operational and system conditions are presented in Section IV. Sections V and VI follow with a general discussion on the findings of this work and overall conclusions, respectively.

II. Theoretical Analysis

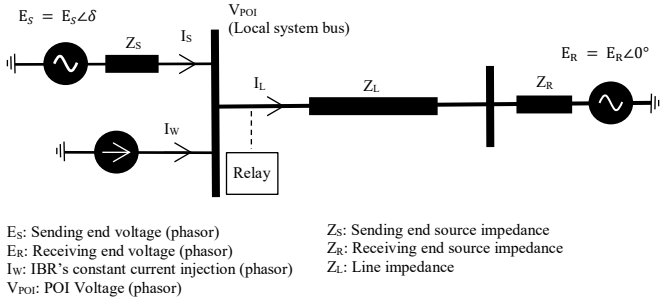

Fig. 1. Simplified single line diagram of the power system during a power swing following a disturbance

Fig. 1 depicts the simplified single line diagram of the power system under investigation, where two conversional synchronous generator based systems (local system represented by a voltage source behind an impedance, E_S/Z_S, and the remote system by E_R/ Z_R) are connected via a transmission line. Z_S and Z_R are transient impedances of the respective sources/systems [11]. An IBR is connected to the bus of the local system, which is its Point of Interconnection (POI). The IBR is represented by a current source, that injects current I_W to the POI. All terms in subsequence equations are phasors unless otherwise stated.

The positive sequence impedance seen by a relay, Z_{Relay}, at the local system bus looking into the transmission line is:

$$Z_{Relay} = \frac{V_{POI}}{I_L} = \frac{E_s - Z_S.I_s}{I_L} \tag{1}$$

Basic circuit equations can be written to determine V_{POI} and I_L in terms of known quantities.

$$\frac{E_s - V_{POI}}{Z_s} = I_s \tag{2}$$

$$I_L = I_S + I_W \tag{3}$$

Using (2) and (3),

$$V_{POI} = E_s - Z_S.(I_L - I_W) \tag{4}$$

Applying the Ohm's law for Z_L and Z_R and using (4), I_L can be expressed as,

$$I_L = \frac{V_{POI} - E_R}{Z_L + Z_R} = \frac{E_s - Z_S.(I_L - I_W) - E_R}{Z_L + Z_R} \rightarrow I_L = \frac{E_s - E_R + I_W.Z_S}{(Z_L + Z_R + Z_S)} \tag{5}$$

Substituting for V_{POI} and I_L in (1) from (4) and (5) respectively, Z_{Relay} can be expressed as,

$$Z_{Relay} = \frac{V_{POI}}{I_L} = \frac{E_s - Z_S.(I_L - I_W)}{I_L} = \frac{E_s}{I_L} - Z_S + \frac{Z_S.I_W}{I_L}$$

$$Z_{Relay} = \frac{(E_s).(Z_L + Z_R + Z_S)}{E_s - E_R + I_W.Z_S} - Z_S + \frac{(Z_S.I_W).(Z_L + Z_R + Z_S)}{E_s - E_R + I_W.Z_S} \tag{6}$$

Taking the remote source to be the angle reference, δ is the phase angle of the local source, θ is the phase angle of the POI, and *'k'* is the ratio of per unit voltage magnitudes of the two sources ($k = |E_S|/|E_R|$), the source and POI voltages phasors can be expressed as:

$$E_S = k.|E_R|\angle\delta, \quad E_R = |E_R|\angle 0, \quad V_{POI} = |V_{POI}|\angle\theta \tag{7}$$

Substituting in (5) and (6),

$$I_L = \frac{k.|E_R|.[cos(\delta) + j.sin(\delta)] - |E_R| + I_W.Z_S}{(Z_L + Z_R + Z_S)} \tag{5-A}$$

$$Z_{Relay} = \frac{k.|E_R|.[cos(\delta) + j.sin(\delta)].(Z_L + Z_R + Z_S)}{k.|E_R|.[cos(\delta) + j.sin(\delta)] - |E_R| + I_W.Z_S} - Z_S + \frac{Z_S.I_W.(Z_L + Z_R + Z_S)}{k.|E_R|.[cos(\delta) + j.sin(\delta)] - |E_R| + I_W.Z_S} \tag{6-A}$$

Assuming that $|E_S|$, $|E_R|$, Z_S, Z_R, Z_L and I_W are known, Z_{Relay} becomes a function of δ, which is the phasor angle of the local source w.r.t. the angle reference.

The magnitude of the IBR's current injection, $|I_W|$, can assumed to be known, however, its phase angle is a function of the voltage at the POI, which in turn is a function of δ. Therefore, finding an elegant solution to V_{POI} is not straightforward. An iterative approach is used to solve for V_{POI} ($= |V_{POI}|\angle\theta$), as a result. The phase angle of V_{POI} can be found as follows.

Using (4), V_{POI} can be expressed as,

$$V_{POI} = E_R + I_L.(Z_L + Z_R) = E_R + \frac{[(E_S - E_R) + I_W.Z_S].(Z_L + Z_R)}{(Z_S + Z_R + Z_L)} \tag{8}$$

If all resistances are neglected, i.e. $Z_S = j|Z_S|$, $Z_R = j|Z_R|$, $Z_L = j|Z_L|$ and the phase angle of I_w with respect to the angle reference is α° ($= \theta + \beta$),

$$|V_{POI}|.[cos(\theta)+jsin(\theta)] = |E_R| + \begin{Bmatrix} k.[cos(\delta)+jsin(\delta)].|E_R| - |E_R| \\ +j.|I_W|.[cos(\alpha)+jsin(\alpha)].|Z_S| \end{Bmatrix}.M_Z \quad (9)$$

where,

$$M_Z = \frac{j.(|Z_L|+|Z_R|)}{j.(|Z_S|+|Z_R|+|Z_L|)}.$$

When the resistances are neglected, M_Z is a scaler. The value of β, which is the phase angle of I_W with respect to V_{POI}, can be assumed known (based on the control strategy). But the value of θ is not known and can be determined considering the operating conditions. Substituting $I_W = |I_W|.[cos(\alpha)+jsin(\alpha)]$ and rearranging (9):

$$|V_{POI}|.[cos(\theta)+jsin(\theta)] - j.M_Z.|I_W|.|Z_S|[cos(\alpha)+jsin(\alpha)] = |E_R| + \{k.[cos(\delta)+jsin(\delta)]-1\}.|E_R|.M_Z \quad (10)$$

$$|V_{POI}|.[cos(\theta)+jsin(\theta)] + M_Z.|I_W|.|Z_S|.[sin(\alpha)-j.cos(\alpha)] = |E_R|.\{1+M_Z.[k.cos(\delta)-1] + j.k.|E_R|.M_Z.sin(\delta)\} \quad (12)$$

Equating real and imaginary parts of (12),

$$|V_{POI}|.cos(\theta) + M_Z.|I_W|.|Z_S|.sin(\alpha) = |E_R|.\{1+M_Z.[k.cos(\delta)-1]\} \quad (13)$$

$$|V_{POI}|.sin(\theta) - M_Z.|I_W|.|Z_S|.cos(\alpha) = k.|E_R|.M_Z.sin(\delta) \quad (14)$$

(13) × $sin(\theta)$:

$$|V_{POI}|.cos(\theta).sin(\theta) + M_Z.|I_W|.|Z_S|.sin(\alpha).sin(\theta) = |E_R|.\{1+M_Z.[k.cos(\delta)-1]\}.sin(\theta)) \quad (15)$$

(14) × $cos(\theta)$:

$$|V_{POI}|.sin(\theta).cos(\theta) - M_Z.|I_W|.|Z_S|.cos(\alpha).cos(\theta) = k.|E_R|.M_Z.sin(\delta).cos(\theta) \quad (16)$$

By subtracting (16) from (15) and applying trigonometric identities, $|V_{POI}|$ can be eliminated to obtain (18):

$$M_Z.|I_W|.|Z_S|.\cos(\theta-\alpha) = |E_R|.\{1+M_Z.[k.cos(\delta)-1]\}.sin(\theta) - k.|E_R|.M_Z.sin(\delta).cos(\theta) \quad (17)$$

$$P_3.cos(\beta) = P_1.sin(\theta) - P_2.cos(\theta) \quad (18)$$

where,

$$P_1 = |E_R|.\{1+M_Z.[k.cos(\delta)-1]\}, \quad P_2 = k.|E_R|.M_Z.sin(\delta), \quad P_3 = M_Z.|I_W|.|Z_S|, \quad \beta = \alpha - \theta$$

If pre-disturbance generator internal voltages remain unchanged and the system impedances are known, the values of P_1, P_2 and P_3 in (18) can be computed for a given set of values for k, δ, $|I_W|$, and β. Then (18) can be solved to determine θ. This allows calculation of the magnitude of V_{POI} using (8). Finally, the positive sequence impedance seen by a relay at the source bus looking into the transmission line can be calculated as:

$$Z_{Relay} = \frac{V_{POI}}{I_L} = \frac{|V_{POI}|\angle\theta.\{j|Z_L| + j|Z_R| + j|Z_S|\}}{|E_s|\angle\delta - |E_R|\angle 0 + |I_W|\angle(\theta+\beta).j|Z_S|} \quad (19)$$

A. Representing the IBR

It is a common practice to represent IBRs using (voltage controlled) current sources in protection studies [16]. The simplified current source representation of the IBR in this study ignores the effects of an interconnection system, which often is a short tie-line between the POM (Point of Measurement) and POI of the IBR. In addition, since active and reactive power requirements of an IBR are defined at the POM (which is the HV side of the main IBR transformer) [12], lumping the entire IBR plant into a current source is a reasonable approximation. For a given steady state operating point, the magnitude and relative phase angle (or power factor) of the IBR's current injection can be assumed to be constant. In this study, unity power factor operation (β=0°) is assumed during the regular operation. During a disturbance, the magnitude of the current injection would not change drastically due to the current limits imposed by power electronic converters of the IBR. However, the phase angle of the injected current may change significantly depending on the severity of the excursion and applicable performance requirements. The key dynamic behavior that can have a significant impact in the context of power swings after a major disturbance is the current injection during voltage ride-through (VRT) mode. This is primarily due to VRT performance requirements which mandate fast enough response to affect power swings (step response < 2.5 cycles and setting time < 4 cycles [12]). Thus, other control and electrical system dynamics are ignored in this simplified analysis. Given in Fig. 2 is an example of positive sequence current injection requirements during VRT operation [6]. The parameter K_{VRT} is the ratio between the per-unitized (positive sequence) reactive current and per-unitized (positive sequence) voltage deviation at POI (the parameter K_{VRT} defines the boundary of minimum requirement).

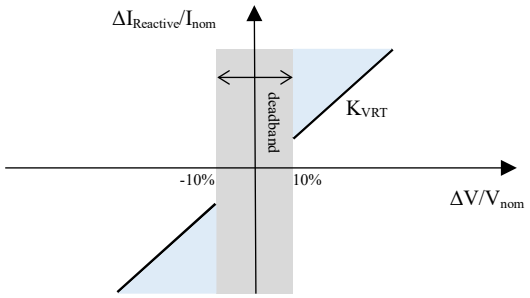

Fig. 2. Example positive sequence current injection requirements during voltage ride-through

It is assumed that the IBR is grid following and can ride through the power swing (at least the first swing). During voltage ride-through operation, priority is given to reactive current injection and any residual current injection capacity will be used for active current and β is set accordingly. During regular operation, priority is given to active current injection. Also, note that only positive sequence reactive current injection is applicable for this investigation as power swings are inherently balanced phenomena.

III. Validation Using EMT Simulations

The accuracy of the theoretical derivations was verified using Electromagnetic Transient (EMT) simulations of the simplified power system shown in Fig. 1. The base-case power system was represented with following parameters: local source impedance Z_S = j0.1 pu, remote source impedance Z_R = j0.15 pu, the line impedance Z_L = j0.1 pu, and the ratio between local and remote source voltage magnitudes k = 1.02. The current injection from the IBR was set to a value corresponding to a system SCR (Short Circuit Ratio) of 10. All per-unit values are in 230 kV and 100 MVA base. Relaying location was at the local end of the transmission line as shown in Fig. 1.

Fig. 3 compares the theoretically calculated results (dotted line) against those obtained from EMT simulations with the slip frequency, which determines the swing speed, set to 0.5 Hz (solid line) and 0.03 Hz (dashed line). The impedances Z_S, Z_R, and Z_L are also shown in the same figure, taking relaying point as the origin. As can be seen from Fig. 3-(a), there is considerable mismatch between the impedance trajectories obtained theoretically (dotted line) and EMT simulations for 0.5 Hz slip speed. This, however, is primarily due to the impact of signal processing (phasor extraction using a DFT function) in the EMT simulation to determine the apparent impedance at the relaying location. In this context, it is worth noting that the theoretical calculations are in phasor domain and as such, have no notion of time (or slip frequency). On the other hand, EMT simulations are performed in time domain and must be transformed into phasor domain for a meaningful comparison using suitable signal processing techniques. This conversion, using signal processing techniques such as DFT based phasor extraction, is inherently associated with delays. During a power swing, the voltage and current measurements (and the apparent frequency to the relay) are in constant change, thus, there is a persistent lag/error between the theoretical values and the phasors extracted at a given moment in time. This is highlighted by the observation that the mismatches are greater at fast moving section of the trajectory ($\delta \approx 0^{\circ}$) and much smaller at slow moving parts of the trajectory ($\delta \approx 180^{\circ}$, Fig. 3-(b)) due to the performance of the DFT algorithm during system dynamics.

A further illustration of this phenomenon is the fact that the mismatches between phasor domain (theoretical) calculations and time-domain simulation results decreased as the slip frequency was reduced in EMT simulation. As can be seen Fig. 3.(a), at 0.03 Hz, the two trajectories are very closely in agreement with one another. It should be noted that a power swing at 0.03 Hz is not realistic, but this exercise was done only for demonstration of the impact of delay and errors due to phasor extraction under continuously varying off-nominal frequency. Irrespective of the mismatches at other sections, the two trajectories exhibited a close match in the range where the pole slipping occurs ($\delta \approx 180^{\circ}$), which is the region of interest for power system protection. Fig. 4 presents a comparison between theoretical and EMT results for different system SCR. Results for SCR values 3, 5, 10 and no IBR are presented and all of them are in close agreement.

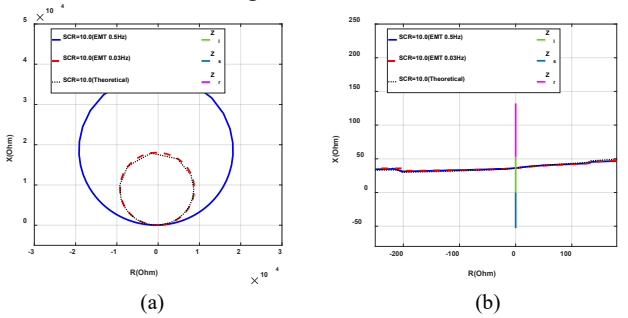

(a) (b)

Fig. 3. Comparison of theoretical and EMT results, (b) zoomed plot with impedances Z_s, Z_l and Z_r.

Given in Fig. 6 is a comparison of results between the theoretical calculation and a more detailed EMT simulation performed in a digital real-time simulator. In this case the IBR was represented using an averaged model with detailed d-q domain controls. The local source was replaced by a conventional synchronous generator (SG), which was represented using a detailed dynamic model (with both rotor and stator dynamics) from the master component library. Fig. 5 provides the parameters (per-unit values are in 400 kV and 222 MVA base) of the power system used for detailed EMT simulations. The effective local source impedance, Z_S, was j0.45 pu and made-up by the summation of the transient impedance of the synchronous generator (X_d') and the leakage impedance of the generator step-up (GSU) transformer. The initial active power flow from the IBR and synchronous generator were approximately 200 MW each. The power swing was triggered by applying a fault and subsequently tripping one of the lines between the generation plant and the remote system. The results in Fig. 6 confirms the validity of the theoretical results, specifically in the region around $\delta \approx 180^{\circ}$. The loop like segment of trajectory is due to the fault clearing transient. The deviations in the other regions are due to the signal processing related issues explained earlier. One can also notice a general similarity in the two sets of EMT simulation results (given in Fig. 3 and Fig. 6).

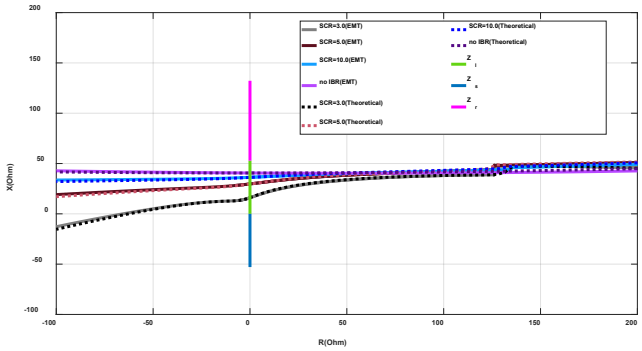

Fig. 4. Comparison of theoretical and EMT results for different system SCR

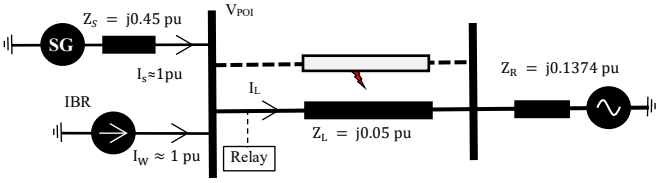

Fig. 5. Simplified single line diagram of power system used for detailed EMT simulations

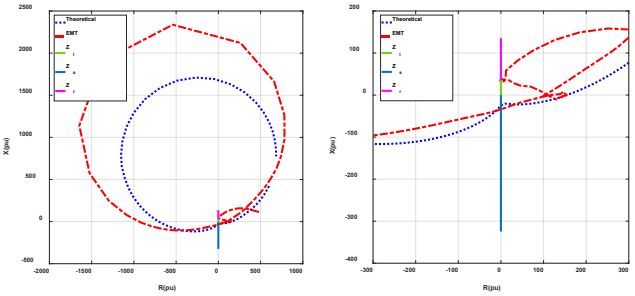

Fig. 6. Comparison of theoretical and detailed EMT simulation results

Similar to previous simulation, three-phase, instantaneous currents and voltages were measured at the relaying location (as indicated in Fig. 5). Signal processing was done using master library relaying components in the simulation tool, which

provided both voltage and current phasors and the positive sequence impedance seen at the relaying location.

Results given in Fig. 3, Fig. 4 and Fig. 6 validate the theoretical equations derived in Section II. The analysis presented in subsequent sections of this paper were carried out using the phasor domain theoretical equations only.

IV. Results

The following sub-sections analyze the influence of different system parameters on the swing impedance trajectories. The impedances Z_S, Z_R, and Z_L are also shown in figures as line segments, when applicable, as a frame of reference.

A. Base Case

Results presented in Fig. 7 compares the swing impedance trajectories of the system described in Section III (base case) for no IBR and base case IBR scenarios. Z_S and Z_R source impedances were selected to be j0.1 pu and j0.15 pu, respectively, whereas Z_L was set at j0.1 pu. The ratio between local and remote source voltage magnitudes was 1.02 pu and the system SCR was set to 10.

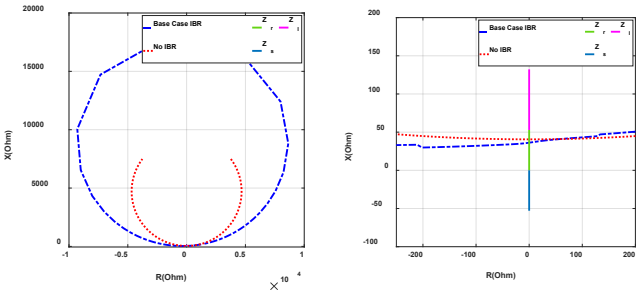

(a) (b)

Fig. 7. (a) Swing impedance trajectories for no-IBR and base-case IBR scenarios, (b) zoomed plot with impedances for Z_s, Z_l and Z_r.

B. Impact of Short Circuit Ratio

SCR is the ratio between of the short circuit level (SCL) of the AC system at the POI and the power rating of the IBR. A higher SCR indicates a stronger AC system and in general, SCR values below 2.5 are considered interconnections to weak AC system. SCR can vary with time depending on the system operating conditions, topology and various other contingencies. Fig. 8 presents swing impedance trajectories of the system for different system SCRs (2.5, 3.0, 5.0, 10.0,12.0) and no IBR. All other system parameters were kept unchanged.

The impact of system SCR on swing impedance trajectories can be separated into two aspects. Firstly, considering the overall trajectories given in Fig. 8-(a), the decrease of SCR (increase of IBR current injection) resulted in inverting the impedance trajectory along the R-axis (from being largely on positive X plain to negative X plain). This is analogous to changing the ratio of local to remote source voltage magnitudes from a value greater than 1 to smaller than 1 (in no-IBR case).

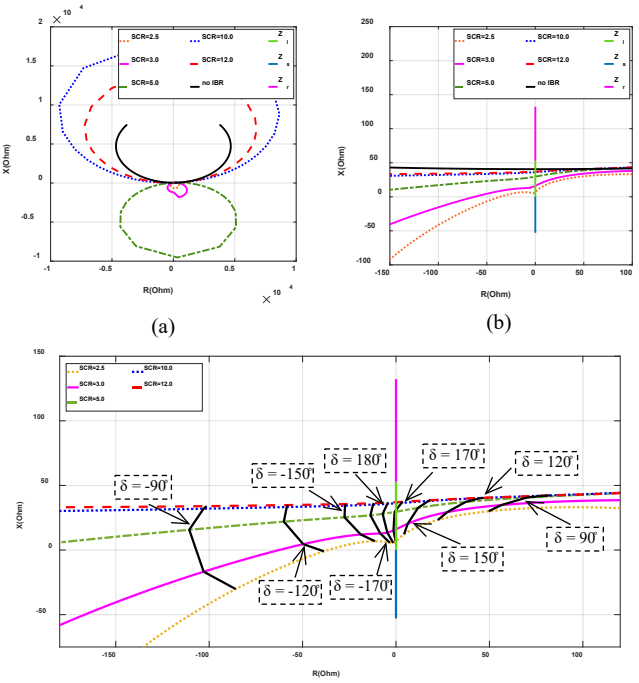

(a) (b)

(c)

Fig. 8. (a) Swing impedance trajectories for different SCR values, (b) zoomed plot with respective line impedance for Z_s, Z_l and Z_r, (c) variation of δ

Given in Fig. 9 are 3-dimensional plots of swing impedance trajectories plotted with δ (R, X, δ) for different SCR values. Notice that δ is wrapped between [-180˚, 180˚] in this plot. Data points shown correspond to δ ≈ 180˚ and indicate that there is a non-zero real part in the impedance when there is a non-zero current injection. From Fig. 8-(b), it can be seen that current injection altered the path of the impedance trajectory when δ ≈ 180˚. In addition, it can be seen that the lower the SCR, higher the deviation of the trajectories from the no IBR case.

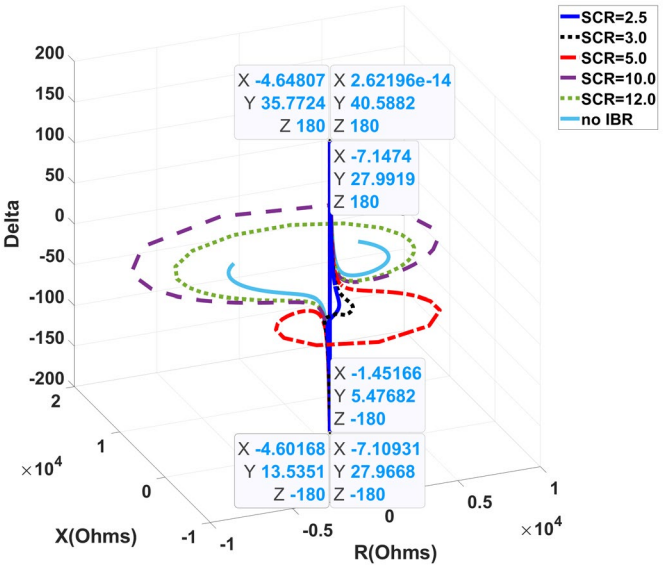

Fig. 9. (a) Swing impedance trajectories plotted with δ for different SCR values; data points correspond to δ=180˚

C. Impact of IBR Active Power Output

Fig. 10 presents the swing impedance trajectories of the system for different active power injections to simulate the

intermittency of a typical IBR. All other system parameters were kept unchanged from the base case. Results for 10%, 30% 50% and 100% active power injection are presented and 100% corresponds to the current injection in the base case.

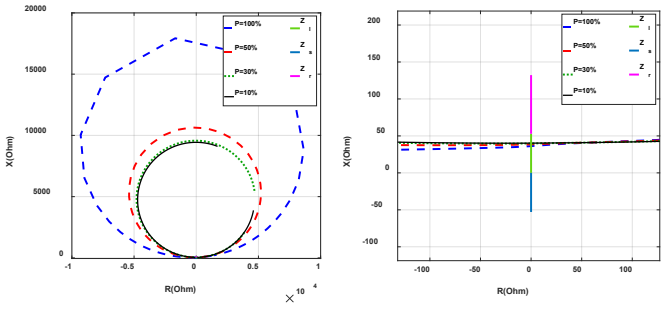

(a) (b)

Fig. 10. (a) Swing impedance trajectories for different active power injection, (b) zoomed plot with respective line impedances for Z_s, Z_l and Z_r.

While the change of active power injection altered the trajectory of the apparent impedance for lower δ values (δ ≈ 0˚), its effect on the trajectory was minimal in δ ≈ 180˚ region.

D. Impact of Source Voltage Magnitudes

Presented in Fig. 11 are swing impedance trajectories of the system for different source voltage magnitudes. The parameter *k* is the magnitude ratio of the local and remote voltage sources, each of which represent two conventional power systems as equivalents. It can be seen that, for cases where $k \geq 1.01$, the trajectories are in the positive X plain and those where $k < 1.01$ were inverted (in the negative X plain). It is known that in conventional systems (without an IBR) k = 1.0 is the boundary case. With these results, it can be said that the presence of the IBR in this system has an effect similar to decreasing the k values in a conventional system without IBRs.

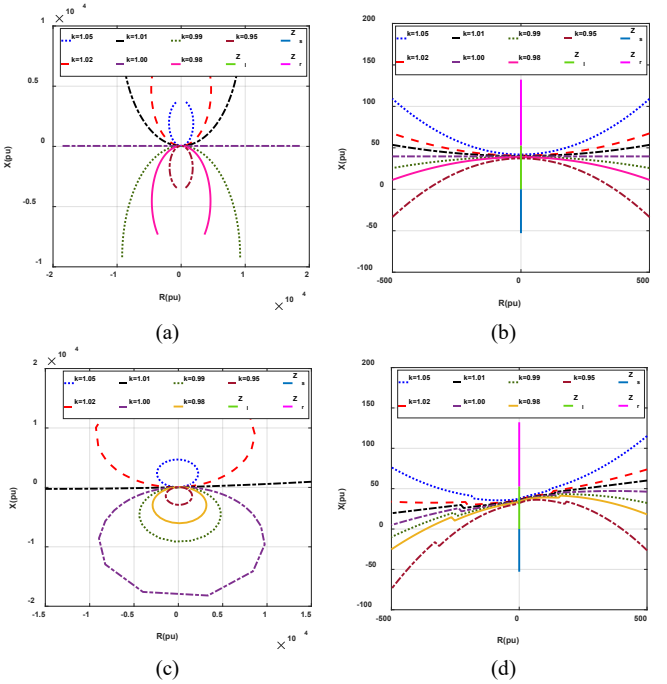

(a) (b)

(c) (d)

Fig. 11. Swing impedance trajectories for different source voltage magnitudes (a) no IBR, (b) zoomed plot of (a), (c) base case IBR, (d) zoomed plot of (c),

E. Impact of Current Injection During Voltage Ride-Through

Most modern IBRs are required to inject reactive current during VRT operation as a performance requirement. Fig. 12 presents the swing impedance trajectories of the system for different levels of (positive sequence) reactive current injections. The parameter K_{VRT} is the ratio between the per-unitized (positive sequence) reactive current and per-unitized (positive sequence) voltage deviation at POI (represents the current injection characteristic). As can be seen from Fig. 12-(a), the three characteristics are identical except for the period where the voltage ride through is activated. The trajectories deviate from one another slightly due to differences of the phase angle of the injected current during VRT operation. This occurs around the valley of the voltage envelop when its magnitude drops below the VRT threshold as the δ approaches 180˚.

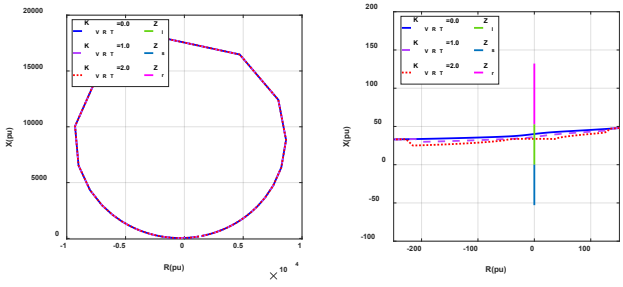

(a) (b)

Fig. 12. (a) Swing impedance trajectories for different levels of reactive current injection during VRT, (b) zoomed plot with respective line impedances for Z_s, Z_l and Z_r.

F. Impact of IBR Type

Presented in Fig. 13 are swing impedance trajectories of the system for different IBR types. The plot compares results for a regular IBR where injection of active power is prioritized, a BESS (Battery Energy Storage System) in charging mode, where absorption of active power is prioritized and a STATCOM, where injection of (leading) reactive power is prioritized. All IBRs were set to have the same current injection capacity.

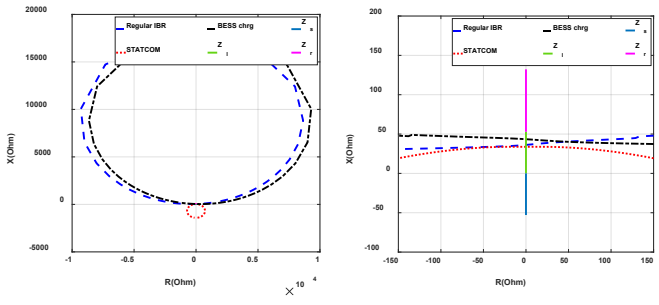

(a) (b)

Fig. 13. (a) Swing impedance trajectories for different IBR types, (b) zoomed plot with respective line impedances for Z_s, Z_l and Z_r.

The regular IBR and BESS cases had the base case scenario VRT current injection, whereas the STATCOM only had reactive current injection (no VRT mode operation). While the trajectories did not change considerably in in the region near δ ≈180˚, the overall swing impedance trajectory for the STATCOM was significantly different (smaller and inverted on the x-axis) from other IRB types.

G. Impact of System Impedances

Fig. 14 presents the swing impedance trajectories for a different combination system impedance. In these tests, line impedance, Z_L and remote source impedance, Z_R were selected to be j0.075 pu and j0.05 pu, respectively. The local source impedance, Z_S was changed across tetes and set at different values varying from at j0.05 to 0.25 pu. All per-unit values are in 230 kV and 100 MVA base. The current injection from the IBR was set to a value corresponding to a system SCR of 5 in all cases.

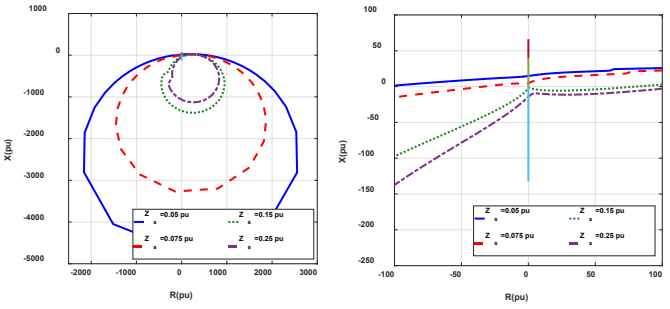

(a) (b)

Fig. 14. (a) Swing impedance trajectories for different source impedances, (b) zoomed plot with respective line impedances for Z_s, Z_l and Z_r.

This exercise was performed to investigate the effects of the AC system parameters on the swing impedance trajectories. Notice that the source impedances are directly correlated to respective system strengths and the line impedance to its length. In addition, the change of Z_S with respect to Z_L can also be viewed as changing the Source to Impedance Ratio (SIR, i.e. the ratio of the source impedance to the line impedance) of the system. In turn, these changes correspond to different system initial conditions (such as power flow) prior to initiation of the power swing. As can be seen from Fig. 14-(b), the point at which the impedance trajectory intersects the Y(reactance)-axis (also the swing center in these cases) goes down with the increment of Z_S. This, however, is to be expected as the increment of Z_S pulls to swing center $[(Z_S+Z_L+Z_R)/2]$ towards the negative Y direction (even without an IBR).

V. Discussion

This section provides an overall discussion on results presents in earlier in this work.

A. Interpretation of Results

Observing (21), which is a rearranged form of (7-B), one can observe that the current injection from the IBR appears in only one of the terms in the equation.

$$Z_{Relay} = \frac{(E_s + Z_S.I_W)}{I_L} - Z_S = \frac{(E_s + Z_S.I_W).(Z_L + Z_R + Z_S)}{(E_s - E_R) + I_W.Z_S} - Z_S \quad (20)$$

$$Z_{Relay} = \frac{(Z_L + Z_R + Z_S)}{[1 - E_R/(E_s + Z_S.I_W)]} - Z_S \quad (21)$$

Considering the base case IBR current injection (SCR 10.0), the term $I_w.Z_s$ is significantly smaller than E_s around $\delta \approx 180^{\circ}$. For example, if we consider the $\delta = 180°$ case, the value of the term $I_w.Z_s$ is $0.14\angle -79.75°$ whereas $E_s = -1.02\,pu$ ($|I_W| = 1.4$ pu, $Z_S = 0.1j$ pu, $E_s\angle 180° \approx -|E_s| = -1.02$ pu) . Therefore, the effect of the IBR current injection (I_w) is small in the region near $\delta \approx 180^{\circ}$. On the other hand, (20) indicates that when δ is small ($\delta \approx 0^{\circ}$), the value of the term $I_w.Z_s$ becomes comparable with the value of $E_S - E_R$ as the two voltage phasors are now more or less in phase cancelling out each other.

Clear example of this outcome can be seen in Fig. 7 where swing impedance trajectories for no IBR and with IBR cases are compared. The deviation between the two trajectories is far greater when δ is small as opposed to higher values of δ, where the two trajectories are much closer. This phenomenon is readily apparent in the most of the other results as well.

B. Implications to Power System Protection

Based on the discussion presented in above Section V-A, one can reason that the effect of an IBR on impedance-based power swings protection is small as swing impedance trajectories seen by a relay are not drastically changed for higher values of δ (poles slip), where power swings protection is applied. On the other hand, having a closer look at results for lower SCR cases (or higher current injections) indicates that the presence of IBRs alters the swing impedance trajectories considerably. This effect may be required to be taken into consideration in setting blinders for power swing blocking (PSB) and out-of-step tripping (OST) for lower SCR systems.

Swing impedance trajectories for SCR=2.5 are given with respective impedances Z_s, Z_l, Z_r, and inner and outer OOS protection blinders in Fig. 15. For example, due to the asymmetry of the trajectory on Y-axis, right and left blinders may have to be set at different distances as opposed setting them at the same distance on either side in a conventional system. Furthermore, actual relays that estimate the impedance using DFT, will see the trajectory similar to those obtained with EMT simulations (the impact of delay and errors due to phasor extraction under continuously varying off-nominal frequency is present for the no IBR scenario too).

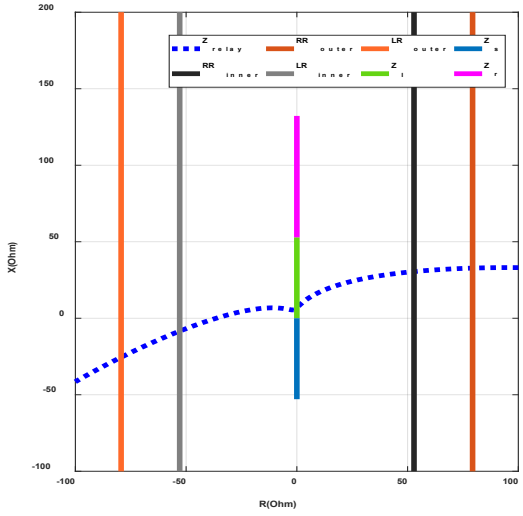

Fig. 15. Swing impedance trajectories for SCR=2.5 plotted with respective line impedance for Z_s, Z_l, Z_r, and inner and outer PSB and OST blinders

C. Benefits and Limitations of the Proposed Model

The work presented in this paper modifies the well-known analysis of power swing protection analysis method

(established for synchronous-machine based systems [1]-[2]) to incorporate IBRs. Using the proposed theoretical model, the behavior of power swing impedance trajectories in a system with IBRs can be approximated with a little effort, in a manner comparable to that of a conventional power system. Typically, power swing protection schemes are configured by performing detailed dynamic simulations considering a many system conditions, configurations and contingencies. While these produce comparatively accurate results, conducting such simulations is resource intensive and they can produce results that are convoluted and difficult to interpret on their own. The theoretical model proposed in this paper offers a generic, easy-to-execute tool that can be used to initialize the settings of a power swing protection scheme (for example, blinder settings), which can then be verified by conducting more complex and detailed dynamic simulations. This model is also useful for preliminary or simplified studies where only a general idea of the behavior of swing trajectories is required and to interpret (or troubleshoot) results for more detailed dynamic simulations.

This method, therefore, provides a convenient and familiar way to incorporate IBRs into out-of-step protection and relaying, which in turn improves design and performance of power system protection. The proposed method also provided a vital point of reference against which results from more detailed simulation can be compared. It is based on few basic assumptions and developed in a generic manner. Its adaptation is quite straightforward and can be implemented using any modern computer coding language with mathematical capabilities.

Finally, it is important to restate that this work is primarily done in phasor domain hence, it has no notion of time (for example, how fast the trajectories move on R-X plain). The whole purpose if this work is to investigate the effect of IBR on electrical (swing impedance) trajectories on the R-X plain. It is intended to be used to analyze the behavior swing impedance trajectories with variation of δ (the phase angle difference between the two sources during the swing). In its current form, this model is not designed be used to study any time-varying behavior. Furthermore, as demonstrated in the paper, the effects of measurement errors, signal processing can cause disagreements between the behavior predicted by the model and that of the real power system. Various system dynamics not considered in the model can also cause discrepancies between the theoretical model and the real power system.

VI. Conclusions

This paper presented a theoretical approach to investigating impedance trajectories during power swings in the presence of IBRs. A variety of different operational and system conditions were investigated during the work presented in this paper. The premise of theoretical analysis presented was also validated by EMT simulations. In addition, a general discussion on the findings of this work including their implications to power system protection and benefits and limitations of the proposed model were also presented. The finding in this work indicates that while swing impedance trajectories did not change significantly in in the region near $\delta \approx 180^{\circ}$ (compared to no IBR case), the overall trajectory may be significantly different depending on the SCR and IBR type. The results also indicated VRT current injection and active power injection level had minimal impact. Based on the finding of the work, it can be reasoned that IBRs do not alter the swing impedance trajectories significantly enough to impact the OOS protection (blinder setting etc.) expect for low SCR systems where the effects of IBRs may be required to be taken into consideration. Future work of this research will look further into IBR dynamics/control modes (for example, grid forming operation) and varied system operating conditions. The proposed method of analysis has merit in determining the effect of IBRs on swing impedance trajectories and can be easily incorporated with phasor-based relay setting investigations.

VII. References

[1] "Power swing and out-of-step considerations on transmission lines," IEEE Power System Relaying and Control Committee (PSRC) Working Group WG-D6, Jul. 2005.

[2] S. H. Horowitz and A. G. Phadke, *Power System Relaying*, 4th Edition, Wiley, 2014.

[3] "Protection System Response to Power Swings," NERC System Protection and Control Subcommittee, August 2013.

[4] Normann Fischer, Gabriel Benmouyal, Daqing Hou, Demetrios Tziouvaras, John Byrne-Finley, and Brian Smyth, "Tutorial on Power Swing Blocking and Out-of-Step Tripping," presented at the 39th Annual Western Protective Relay Conference, Spokane, Washington, Oct. 2012.

[5] Joe Mooney and Normann Fischer, "Application Guidelines for Power Swing Detection on Transmission Systems," presented at the 42nd Annual Minnesota Power Systems Conference, Saint Paul, Minnesota, Nov. 2006.

[6] "Protection Challenges and Practices for Interconnecting Inverter Based Resources to Utility Transmission Systems" IEEE Power System Relaying and Control Committee Report of Working Group C32 of the System Protection Subcommittee, Sep 2020.

[7] A. Haddadi, E Farantatos, I Kocar, U Karaagac, "Impact of inverter-based resources on system protection" *Energies*, vol. 14, no. 4, 2021.

[8] A. Haddadi, I. Kocar, U. Karaagac, H. Gras and E. Farantatos, "Impact of Wind Generation on Power Swing Protection," in *IEEE Transactions on Power Delivery*, vol. 34, no. 3, pp. 1118-1128, June 2019, doi: 10.1109/TPWRD.2019.2896135.

[9] Amin Jalilian and Duane A. Robinson. "Impact of Inverter-Based Resources on Transmission Line Relaying-Part II: Power Swing Protection." *Frontiers in Electronics* 4: 1144383

[10] M. Jayamohan, S. Das and S. Brahma, "Impedance Trajectories during Stable and Unstable Power Swings in Presence of PQ Control based PV Generations," 2023 IEEE Power & Energy Society General Meeting (PESGM), Orlando, FL, USA, 2023, pp. 1-5, doi: 10.1109/PESGM52003.2023.10253031.

[11] P. S. Kundur and O. P. Malik, *Power System Stability and Control*, 2nd Edition, McGraw Hill, 2022.

[12] "IEEE Standard for Interconnection and Interoperability of Inverter-Based Resources (IBRs) Interconnecting with Associated Transmission Electric Power Systems," in IEEE Std 2800-2022, vol., no., pp.1-180, 22 April 2022.

[13] M. -A. Nasr and A. Hooshyar, "Power Swing in Systems with Inverter-Based Resources—Part I: Dynamic Model Development," in *IEEE Transactions on Power Delivery*, vol. 39, no. 3, pp. 1889-1902, June 2024, doi: 10.1109/TPWRD.2024.

[14] M. -A. Nasr and A. Hooshyar, "Power Swing in Systems with Inverter-Based Resources—Part II: Impact on Protection Systems," in *IEEE Transactions on Power Delivery*, vol. 39, no. 3, pp. 1903-1917, June 2024, doi: 10.1109/TPWRD.2024.

[15] Xiong, Yongxin, Heng Wu, Xiongfei Wang, and Yifei Li. "Efficacy Analysis of Pow-er Swing Blocking and Out-of-Step Tripping Functions in Grid-Following VSC Sys-tems." arXiv preprint arXiv:2311.05247 (2023).

[16] "Modification of commercial fault calculation programs for wind turbine generators," IEEE Power System Relaying and Control Committee Report of Working Group C24 of the System Protection Subcommittee, July. 2020.